

Article

Capacity Analysis of Power Beacon-Assisted Industrial IoT System with UAV Data Collector

Aleksandra Cvetković^{1,*}, Vesna Blagojević² and Jelena Manojlović¹¹ Faculty of Mechanical Engineering, University of Niš, 18000 Niš, Serbia² School of Electrical Engineering, University of Belgrade, 11000 Belgrade, Serbia* Correspondence: aleksandra.cvetkovic@masfak.ni.ac.rs

Abstract: The performance analysis of an energy constrained Internet of Things (IoT) system with unmanned aerial vehicle (UAV) is provided in this paper. In the considered system, a power beacon is used for the energy supply of a sensor node that has no other power sources, while the UAV is used for the collection of sensor data. The outage and capacity performances are analyzed under the assumption of a Nakagami- m fading environment, for the case when the power and information transfer are performed based on the time-switching protocol and the UAV is randomly positioned at a certain height. Based on the provided analysis we derive the exact closed-form expressions for the outage probability, the outage capacity and the ergodic capacity of the power beacon assisted IoT system. The analytical results are confirmed using an independent simulation method. The performed analysis demonstrates the impact of various system and channel parameters on system performances.

Keywords: data collecting; energy harvesting; industrial sensor network; Internet of Things (IoT); outage probability; outage capacity; power beacon; unmanned aerial vehicles (UAV)



Citation: Cvetković, A.; Blagojević, V.; Manojlović, J. Capacity Analysis of Power Beacon-Assisted Industrial IoT System with UAV Data Collector. *Drones* **2023**, *7*, 146. <https://doi.org/10.3390/drones7020146>

Academic Editors: Emmanouel T. Michailidis, Demosthenes Vouyioukas and Petros Bithas

Received: 27 December 2022

Revised: 12 February 2023

Accepted: 19 February 2023

Published: 20 February 2023



Copyright: © 2023 by the authors. Licensee MDPI, Basel, Switzerland. This article is an open access article distributed under the terms and conditions of the Creative Commons Attribution (CC BY) license (<https://creativecommons.org/licenses/by/4.0/>).

1. Introduction

It is well known that the usage of a wireless sensor network (WSN) tends to be an essential enabler of numerous applications related with infrastructure monitoring and surveillance, medical care, smart home, environment monitoring, etc. [1–4]. Furthermore, it contributes to automation process development in Internet of Things (IoT) systems within Industry 4.0. [5–9]. These applications can be easily implemented in dense urban areas where data collecting is facilitated by a wide range of available infrastructure. However, in numerous scenarios, the sensor network has to be set in an environment where the infrastructure is hardly available. In that case it is essential to provide a robust energy power supply, as the positions of the sensor network nodes might be inaccessible, and the reliance on frequent battery replacement is impractical. Various existing natural energy sources could be used for enabling energy needed for the communication purposes, since the sensor nodes are low-power [10]. The main disadvantage is that these sources are not reliable as they depend on unpredictable circumstances such as weather conditions, etc. As simultaneous information and power transfer (SWIPT) represents an appealing technology for various applications within contemporary communication systems, various solutions for its implementation have been investigated [11–13]. One of the possible feasible approaches is the use of the dedicated node for the wireless power supply of locally positioned sensor nodes [14,15]. The application of SWIPT with power beacon (PB) in hierarchical WSN is analyzed in [16]. The PB can be used for the enabling of energy for sensor nodes as well as the powering of access points in cellular networks, as is shown in [17]. As the usage of millimetre waves for signal transmission is one of the key technologies for 5G networks and applications, the millimetre wave ad hoc networks with the PB assistance and the influence of the transmit power of PB on the coverage probabilities of network are analyzed in [18].

The implementation of wireless sensor networks can be required in remote and hardly accessible or toxic areas in an uninhabited or industrial environment, where it is challenging

to provide a reliable data collection system. Moreover, in areas that are under risk of natural disasters, special attention should be placed on data collection system design in the case when conventional power and communication infrastructure is destroyed. The energy harvesting framework designed for the emergency and disaster scenarios with an aim to prolong the lifetime of the network using cluster heads that act as relay stations that transfer both information and power signals from a base station to users is proposed in [19]. However, the usage of unmanned aerial vehicles (UAVs) can be also very useful in variable environments [20], as it offers numerous advantages such as the possibility of providing mobile data collectors that can be used in special monitored areas that are not easily approachable or not convenient for ground-based data collectors. For such purposes, one or more UAVs that compose Flying Ad Hoc Networks, FANET, can be used [21]. In [22], the novel cluster-based mechanism in FANET is proposed for the Nakagami- m fading scenario and the performance improvement is demonstrated. Moreover, if a sensor network is deployed over a large area, the UAV can contribute to faster search and lower energy consumption of sensor nodes. This is due to the fact that the usage of UAVs can enable data collection with shorter propagation paths between the transmitter and the receiver, thus reducing path losses. Therefore, the employment of UAV for data collection leads to lower latency, as well as higher reliability and quality of service (QoS) [20,23].

1.1. Related Literature

In this subsection, we provide the survey of the related published studies. The usage of UAVs for data collecting purposes is analyzed in [20], while a special application for disaster recovery scenarios is presented in [24]. The new channel model of the UAV-based communication system that encompasses various fading and shadowing effects is proposed in [25], whereas outage, error and capacity performance are additionally studied. The impact of the ground user mobility and channel fading on the outage performances of the system employing the static multicopter UAV is analyzed in [26]. An outage performance analysis of hybrid satellite–terrestrial network with UAVs employed as decode-and-forward relays is provided in [27], under the assumption that UAVs are randomly positioned in a 3D cylindrical area. The capacity maximization of the UAV communication system applying non-orthogonal multiple access (NOMA) at downlink is analyzed in [28]. Performances of the IoT network with energy-limited UAV relay and applied downlink NOMA strategy are investigated in [29], for the Nakagami- m fading environment and different employed relaying schemes. A system architecture with specialized UAVs used for wireless energy transfer applied for the recharging of other UAVs is proposed in [30], and both the flying times of the rechargeable UAVs and the energy transfer gain are optimized. The application of energy harvesting in a UAV-assisted half-duplex relay IoT system is studied in [31], for the Nakagami- m fading environment and the impact of interference on the outage performances is considered. The emergency communication in disaster recovery network using UAV-based relaying is investigated in [32], where resource allocation and UAV trajectory are optimized in order to maximize the number of IoT devices. New rate-splitting multiple access in the system in which a UAV is used as a base station is investigated in [33] and the outage probability and corresponding throughput are derived under the assumption of Nakagami- m fading channel statistics. In [34], the scenario where UAVs act as a multiple base station hovering at a fixed horizontal position and fixed altitude to serve for both energy supply and relaying information transmission for end users is analyzed, and the optimization of the beamwidth, the transmit power and the energy harvesting time coefficients are provided. In [35], a scenario in which UAV node has both functions of data collecting and energy supply for IoT nodes is considered. The UAV sends energy to IoT nodes, which is afterwards used for data transfer to the UAV data collector. The security aspect of information transfer in an IoT system assisted with UAV for the purpose of data collecting is analyzed in [36], for the Rice and Rayleigh propagation environment model and for the scenarios when line-of-sight (LOS) and non-line-of-sight propagation occur, respectively.

Finally, for all considered applications, UAV flight parameters must comply with the existing regulative framework, and this issue is analyzed in detail in [37,38].

1.2. Motivation and Contribution

Due to their wide applicability, power beacon-assisted wireless sensor networks have already been analyzed for various scenarios, as shown in the previous subsection. In this paper, we present the performance analysis of the wireless sensor network with the ground-based power beacon. Differently from previously published papers, the UAV is utilized for data collection in an energy-constrained wireless sensor network. The motivation for this type of system is its importance for industrial applications in the cases where the ground-based power supply nodes can be enabled, but due to the inaccessibility of the telecommunication infrastructure in the area, the ground-based data collecting system represents an issue. To fill this gap, we analyze a PB-assisted wireless sensor network where data collecting is realized with the help of the UAV. Although energy-constrained UAVs are also analyzed in the recent literature [30,31], in this manuscript we assume that sensor network in industrial area is energy limited, while the UAV dedicated for data collecting has enough energy for the intended purpose, as in [34]. The system performances are analyzed under the general assumption that the fading in the propagation environment is subject to Nakagami- m distribution, due to the fact that this distribution encompasses various channel fading scenarios as special cases. For specified values of parameter m , Nakagami- m distribution includes Rayleigh distribution (for $m = 1$), and nonfaded additive white Gaussian noise (AWGN) channel model (for $m \rightarrow \infty$). Furthermore, it closely approximates Rician ($m > 1$) as well as Hoyt ($m < 1$) distribution [39,40]. Large values of m refers to the less-severe fading conditions. In our study we assume the UAV is hovering in the circular area, where it is randomly positioned [41]. The stochastic analysis of UAV coverage has been already presented in [42], but the wireless power supply of nodes is not considered. In this paper, we assume that power transfer from the beacon to the IoT sensor and further information transfer to the UAV data collector is performed according to the time-switching (TS) protocol. We assume further that the IoT node is in active transmission mode and sends information to the UAV, which is uniformly randomly positioned within a circle of a certain radius at a given height. Hence, the contribution of this paper is as follows:

- (1) We consider a novel system by incorporating detailed mathematical and simulation analysis. Derived analytical expressions are corroborated by an independent simulation model.
- (2) The novel closed-form expressions for the outage probability and outage capacity of the system are derived.
- (3) The analytical result for ergodic capacity is derived in the exact closed-form.
- (4) Based on the obtained analytical and simulation results we demonstrate the characteristics of the network for various system parameters and propagation conditions including the randomness of the UAV locations. Those results can be used as a guidance for the design of UAV data collection system in inaccessible area.

Our system model can be used in industrial zones where access to IoT sensors is difficult, and the UAV provides the collection of information from the sensors. Furthermore, the considered system model and given performance analysis can be used in natural disaster scenarios such as floods or earthquakes, when the UAV is randomly distributed in the circular disaster area and has a roll of data-collection stations.

2. System and Channel Model

In this paper we analyze the system where the sensor node does not have its own energy sources and it is supplied with the assistance of the power beacon. We investigate outage and capacity performances of the system under the assumption that the propagation environment can be described using the Nakagami- m fading model. It is well known that it represents a general fading model, which incorporates Rayleigh and Rician fading as special cases [40]. It is assumed that the UAV is hovering in the circular area defined by [41],

where it is randomly positioned. The IoT sensor node transfers information to the UAV data collector according to the TS protocol.

The system presented in Figure 1 is composed of an IoT sensor (S) and a power beacon (PB) that is used for sensor node power supply, as the sensor node has no alternative energy sources (such as batteries, for example). As the sensor network is positioned in an inaccessible area, a UAV is used to collect the information from the sensor node. It is assumed that during the collecting time interval, the UAV is positioned at a height H and its position is random within a circle of radius R above the sensor node. The fading envelopes in the channels from the PB to the source and from the source to the UAV are denoted by h_1 and h_2 , respectively, while the corresponding distances between the nodes are equal d_1 and d_2 . The path loss coefficients in the channels from the PB to the source and from the source to the UAV are denoted by δ_1 and δ_2 , respectively.

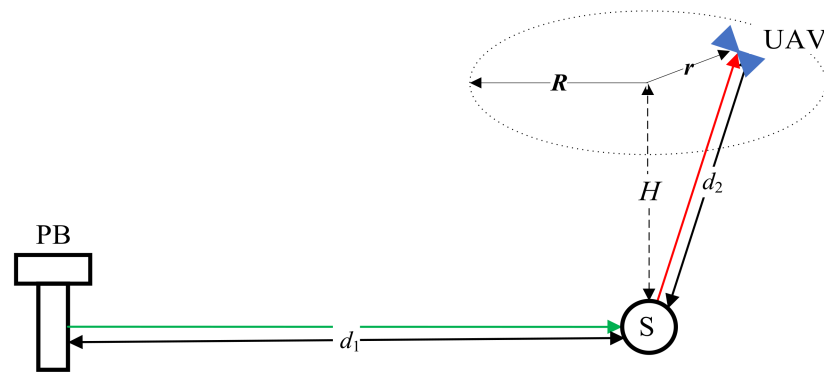


Figure 1. IoT system model with UAV based data collector.

The sensor harvests the RF energy transmitted from the PB based on TS protocol and further uses the accumulated energy to transmit information to the UAV. According to the protocol, within the transmission block time of duration T , the sensor harvests the RF energy from the PB during the first part αT , $0 \leq \alpha < 1$, while the remaining time duration equal $(1 - \alpha)T$ is used to transmit signals to the UAV, as is shown in Figure 2.

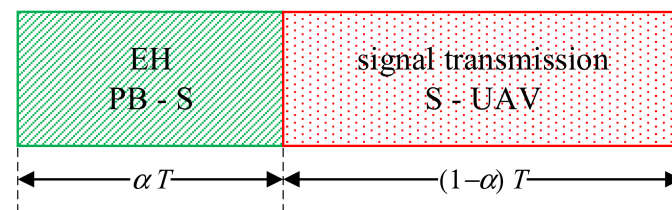


Figure 2. EH and information transmission intervals within total block time T .

The total harvested energy at the sensor during the time interval αT is given by

$$E_H = \eta \frac{P_B \gamma_1}{d_1^{\delta_1}} \alpha T, \tag{1}$$

where P_B is the transmit power of the beacon, $\gamma_1 = |h_1|^2$ denotes the channel power gain between the PB and the sensor, while η ($0 < \eta < 1$) denotes the efficiency of the energy conversion.

It is further assumed [43] that all energy harvested within one time frame is used for the information transmission. Therefore, the sensor transmits the information signal s with the power P_S that is equal

$$P_S = \frac{E_H}{(1 - \alpha)T} = \frac{\eta \alpha}{(1 - \alpha)} \frac{P_B}{d_1^{\delta_1}} \gamma_1. \tag{2}$$

The received information signal at the UAV can be expressed as

$$y_{UAV} = \sqrt{\frac{P_S}{d_2^{\delta_2}}} h_2 s + n, \tag{3}$$

where n is the AWGN component at the UAV with the power σ^2 . The received signal-to-noise ratio (SNR) at the UAV is then given by

$$\gamma_{UAV} = \frac{P_S}{d_2^{\delta_2} \sigma^2} \gamma_2. \tag{4}$$

where γ_2 is the channel power gain of the sensor to the UAV channel, $\gamma_2 = |h_2|^2$. Further, combining previous expression with Equation (2) it can be also written in the following form

$$\gamma_{UAV} = \frac{\eta \alpha}{(1 - \alpha)} \frac{P_B}{d_1^{\delta_1} d_2^{\delta_2} \sigma^2} \gamma_1 \gamma_2. \tag{5}$$

In order to describe the various channel environments, the fading envelopes are modelled by the Nakagami- m distribution with mean values $\bar{\gamma}_i = E\{\gamma_i\}$, $i = 1, 2$, while corresponding channel gains γ_i , $i = 1, 2$ are subject to Gamma distribution with probability density function (PDF) being equal

$$p_{\gamma_i}(\gamma) = \frac{m_i^{m_i}}{\bar{\gamma}_i^{m_i} \Gamma(m_i)} \gamma^{m_i-1} \exp\left(-\frac{m_i \gamma}{\bar{\gamma}_i}\right), \tag{6}$$

where $\Gamma(\cdot)$ denotes Gamma function [44] (Equation (8.31)).

For the observed system and a certain fixed position of the UAV, the PDF of the instantaneous SNR at the UAV, defined by (5), can be calculated combining equations [45] ((7–46) and (5–7)) and using [44] (3.471.9). The PDF represents the generalized K distribution [46,47] and can be expressed in the following form

$$p_{UAV}(\gamma) = \frac{2}{\Gamma(m_1)\Gamma(m_2)} \left(\frac{(1-\alpha)m_1m_2d_1^{\delta_1}d_2^{\delta_2}\sigma^2}{\bar{\gamma}_1\bar{\gamma}_2\eta\alpha P_B} \right)^{\frac{m_1+m_2}{2}} \gamma^{\frac{m_1+m_2}{2}-1} \times K_{-m_1+m_2} \left(2\sqrt{\frac{(1-\alpha)m_1m_2d_1^{\delta_1}d_2^{\delta_2}\sigma^2\gamma}{\bar{\gamma}_1\bar{\gamma}_2\eta\alpha P_B}} \right), \tag{7}$$

where $K_\beta(\cdot)$ is the β -th order modified Bessel function of the second kind [44] (8.432.3).

SNR Statistics of UAV with Random Location

In order to collect the information from the sensor, the UAV is located in the flying area that represents a circle with radius R at the height H . The origin of the circle is centered directly above the sensor and the UAV distance from the circle origin equal r is uniformly distributed according to the following PDF [27]

$$p_r(r) = \frac{2}{R^2} r. \tag{8}$$

Further, the distance between the sensor and the UAV can be expressed as $d_2 = \sqrt{H^2 + r^2}$, so the conditional PDF of the instantaneous SNR at the UAV on r , can be expressed using (7) as

$$p_{UAV}(\gamma|r) = \frac{2}{\Gamma(m_1)\Gamma(m_2)} \left(\frac{(1-\alpha)m_1m_2d_1^{\delta_1}(H^2+r^2)^{\delta_2/2}\sigma^2}{\bar{\gamma}_2\bar{\gamma}_1\eta\alpha P_B} \right)^{\frac{m_1+m_2}{2}} \times \gamma^{\frac{m_1+m_2}{2}-1} K_{-m_1+m_2} \left(2\sqrt{\frac{(1-\alpha)m_1m_2d_1^{\delta_1}(H^2+r^2)^{\delta_2/2}\sigma^2\gamma}{\bar{\gamma}_1\bar{\gamma}_2\eta\alpha P_B}} \right). \tag{9}$$

The PDF of the instantaneous SNR at the UAV is obtained by averaging the conditional distribution given by (9) over the random variable r with PDF defined in (8) which results in the following expression

$$p_{UAV}(\gamma) = \int_0^R p_{UAV}(\gamma|r)p_r(r)dr. \tag{10}$$

After mathematical manipulations given in detail in Appendix A, the PDF of the instantaneous SNR at the UAV is obtained in the following closed form

$$p_{UAV}(\gamma) = \frac{2}{\Gamma(m_1)\Gamma(m_2)} \left(\frac{(1-\alpha)m_1m_2d_1^{\delta_1}\sigma^2}{\bar{\gamma}_1\bar{\gamma}_2\eta\alpha P_B} \right)^{\frac{m_1+m_2}{2}} \gamma^{\frac{m_1+m_2}{2}-1} \frac{1}{\delta_2 R^2} \times \left((H^2 + R^2)^{\frac{\delta_2}{2} \left(\frac{m_1+m_2}{2} + \frac{2}{\delta_2} \right)} G_{1,3}^{2,1} \left(\frac{(1-\alpha)m_1m_2d_1^{\delta_1}\sigma^2\gamma}{\bar{\gamma}_1\bar{\gamma}_2\eta\alpha P_B} (H^2 + R^2)^{\frac{\delta_2}{2}} \middle| \frac{1 - \frac{m_1+m_2}{2} - \frac{2}{\delta_2}}{\frac{m_2-m_1}{2}, \frac{m_1-m_2}{2}, -\frac{m_1+m_2}{2} - \frac{2}{\delta_2}} \right) - H^{\delta_2 \left(\frac{m_1+m_2}{2} + \frac{2}{\delta_2} \right)} G_{1,3}^{2,1} \left(\frac{(1-\alpha)m_1m_2d_1^{\delta_1}\sigma^2\gamma}{\bar{\gamma}_1\bar{\gamma}_2\eta\alpha P_B} H^{\delta_2} \middle| \frac{1 - \frac{m_1+m_2}{2} - \frac{2}{\delta_2}}{\frac{m_2-m_1}{2}, \frac{m_1-m_2}{2}, -\frac{m_1+m_2}{2} - \frac{2}{\delta_2}} \right) \right). \tag{11}$$

3. Ergodic and Outage Capacity

In this section we present the concise analysis of the ergodic and the outage capacity of the observed system given in two following subsections. In the first subsection we present the analysis of the ergodic capacity, that represents important metric for the applications with no delay limitations. In the second subsection, we provide the analysis of outage capacity, applicable for delay-limited scenarios [40].

3.1. Outage Capacity and Throughput

In the following part we derive the exact closed-form expression for the outage probability of the UAV data collecting system that is defined as

$$P_{out}(\gamma_{th}) = F_{UAV}(\gamma_{th}) = \int_0^{\gamma_{th}} p_{UAV}(\gamma)d\gamma. \tag{12}$$

It is well known that it represents the important performance metric and leads to the solution for the throughput analysis. Therefore, by substituting the derived Equation (11) in the definition (12), the outage probability expression is derived in the exact closed-form using [48] (07.34.21.0084.01) as

$$P_{out}(\gamma_{th}) = \frac{2\gamma_{th}^{\frac{m_1+m_2}{2}}}{\Gamma(m_1)\Gamma(m_2)\delta_2 R^2} \left(\frac{(1-\alpha)m_1m_2d_1^{\delta_1}\sigma^2}{\bar{\gamma}_1\bar{\gamma}_2\eta\alpha P_B} \right)^{\frac{m_1+m_2}{2}} \left((H^2 + R^2)^{\frac{\delta_2}{2} \left(\frac{m_1+m_2}{2} + \frac{2}{\delta_2} \right)} \times G_{2,4}^{2,2} \left(\frac{(1-\alpha)m_1m_2d_1^{\delta_1}\sigma^2\gamma_{th}(H^2+R^2)^{\frac{\delta_2}{2}}}{\bar{\gamma}_1\bar{\gamma}_2\eta\alpha P_B} \middle| \frac{1 - \frac{m_1+m_2}{2}, 1 - \frac{m_1+m_2}{2} - \frac{2}{\delta_2}}{\frac{m_2-m_1}{2}, \frac{m_1-m_2}{2}, -\frac{m_1+m_2}{2} - \frac{2}{\delta_2}, -\frac{m_1+m_2}{2}} \right) - H^{\delta_2 \left(\frac{m_1+m_2}{2} + \frac{2}{\delta_2} \right)} G_{2,4}^{2,2} \left(\frac{(1-\alpha)m_1m_2d_1^{\delta_1}\sigma^2\gamma_{th}H^{\delta_2}}{\bar{\gamma}_1\bar{\gamma}_2\eta\alpha P_B} \middle| \frac{1 - \frac{m_1+m_2}{2}, 1 - \frac{m_1+m_2}{2} - \frac{2}{\delta_2}}{\frac{m_2-m_1}{2}, \frac{m_1-m_2}{2}, -\frac{m_1+m_2}{2} - \frac{2}{\delta_2}, -\frac{m_1+m_2}{2}} \right) \right). \tag{13}$$

Furthermore, the outage capacity can be evaluated using

$$C_{out} = \frac{1}{\ln 2} (1 - P_{out}(\gamma_{th})) \ln(1 + \gamma_{th}), \tag{14}$$

while the corresponding throughput is given by

$$T_{out} = (1 - \alpha)C_{out}. \tag{15}$$

3.2. Ergodic Capacity and Throughput

The ergodic capacity represents the maximum achievable rate averaged over various fading states. Therefore, based on SNR distribution at the UAV, the ergodic capacity can be obtained as

$$C_{erg} = \frac{1}{\ln 2} \int_0^\infty \ln(1+x) p_{UAV}(x) dx. \tag{16}$$

Further, by representing natural logarithm function using Meijer’s G-function based on [48] (01.04.26.0003.01) and substituting (11) in (16), the following equation is obtained

$$C_{erg} = \frac{1}{\ln 2} \frac{2}{\Gamma(m_1)\Gamma(m_2)} \frac{1}{\delta_2 R^2} \left(\frac{(1-\alpha)m_1 m_2 d_1^{\delta_1} \sigma^2}{\bar{\gamma}_1 \bar{\gamma}_2 \eta \alpha P_B} \right)^{\frac{m_1+m_2}{2}} \times \left((H^2 + R^2)^{\frac{\delta_2}{2} \left(\frac{m_1+m_2}{2} + \frac{2}{\delta_2} \right)} \int_0^\infty x^{\frac{m_1+m_2}{2}-1} G_{1,3}^{2,1} \left(\frac{(1-\alpha)m_1 m_2 d_1^{\delta_1} \sigma^2 x}{\bar{\gamma}_1 \bar{\gamma}_2 \eta \alpha P_B} (H^2 + R^2)^{\frac{\delta_2}{2}} \middle| \frac{1 - \frac{m_1+m_2}{2} - \frac{2}{\delta_2}}{\frac{m_2-m_1}{2}, \frac{m_1-m_2}{2}, -\frac{m_1+m_2}{2} - \frac{2}{\delta_2}} \right) G_{2,2}^{1,2} \left(x \middle| \begin{matrix} 1, 1 \\ 1, 0 \end{matrix} \right) dx \right. \\ \left. - H^{\delta_2 \left(\frac{m_1+m_2}{2} + \frac{2}{\delta_2} \right)} \int_0^\infty x^{\frac{m_1+m_2}{2}-1} G_{1,3}^{2,1} \left(\frac{(1-\alpha)m_1 m_2 d_1^{\delta_1} \sigma^2 x}{\bar{\gamma}_1 \bar{\gamma}_2 \eta \alpha P_B} H^{\delta_2} \middle| \frac{1 - \frac{m_1+m_2}{2} - \frac{2}{\delta_2}}{\frac{m_2-m_1}{2}, \frac{m_1-m_2}{2}, -\frac{m_1+m_2}{2} - \frac{2}{\delta_2}} \right) G_{2,2}^{1,2} \left(x \middle| \begin{matrix} 1, 1 \\ 1, 0 \end{matrix} \right) dx \right). \tag{17}$$

Finally, applying [48] (07.34.21.0011.01) in (17), the exact closed-form analytical expressions for the ergodic capacity is obtained as

$$C_{erg} = \frac{1}{\ln 2} \frac{2}{\Gamma(m_1)\Gamma(m_2)} \frac{1}{\delta_2 R^2} \times \left((H^2 + R^2) G_{5,3}^{2,4} \left(\frac{\bar{\gamma}_1 \bar{\gamma}_2 \eta \alpha P_B}{(1-\alpha)m_1 m_2 d_1^{\delta_1} \sigma^2 (H^2 + R^2)^{\frac{\delta_2}{2}}} \middle| \begin{matrix} 1, 1, 1 - m_2, 1 - m_1, 1 + \frac{2}{\delta_2} \\ 1, \frac{2}{\delta_2}, 0 \end{matrix} \right) \right. \\ \left. - H^2 G_{5,3}^{2,4} \left(\frac{\bar{\gamma}_1 \bar{\gamma}_2 \eta \alpha P_B}{(1-\alpha)m_1 m_2 d_1^{\delta_1} \sigma^2 H^{\delta_2}} \middle| \begin{matrix} 1, 1, 1 - m_2, 1 - m_1, 1 + \frac{2}{\delta_2} \\ 1, \frac{2}{\delta_2}, 0 \end{matrix} \right) \right). \tag{18}$$

Then, the achievable throughput is given by

$$T_{erg} = (1 - \alpha) C_{erg}. \tag{19}$$

4. Numerical Results

In the following part the important system performance metrics are analyzed and their dependence on the system and channel parameters are examined. In order to demonstrate the accuracy of the derived analytical expressions, the results are corroborated with the results obtained by an independent simulation method. The obtained results are presented in the Figures 3–12. For the channel from the PB to the source and from the source to the UAV the fading envelope waveform sequences with $N = 10^8$ samples are generated. Then, the analyzed performance metrics are evaluated by averaging over successive channel realizations. The obtained numerical results are compared with the derived analytical expressions for the outage probability, the outage capacity and the ergodic capacity given by expressions (13), (15) and (19), respectively. The parameters used for the analytical and simulation results are $P_B = 30$ dBmW, $m_1 = 2.1$, $m_2 = 2.8$, $\delta_1 = \delta_2 = 2.7$, $\eta = 0.9$, $\sigma^2 = 10^{-8}$ mW, unless otherwise indicated in the figures.

In Figure 3 we present the dependence of the outage probability on the height H and the size R of the circular area where the UAV is randomly positioned. It can be observed that the outage probability increases for larger height values. This is in accordance with the expectations as the raise of the height value directly increases the instantaneous distance between the sensor and the UAV and the corresponding path losses. Further, if the UAV is uniformly distributed within the circular shaped area of a larger radius it will be more often located at the positions farther from the sensor, resulting in the larger instantaneous sensor-to-UAV distances and the higher propagation losses. The influence of the surface size on the outage performance is more noticeable when the UAV is positioned at a lower height. In that case, the increase of R has dominant influence on the increase of the distance d_2 , and therefore on the system performance degradation.

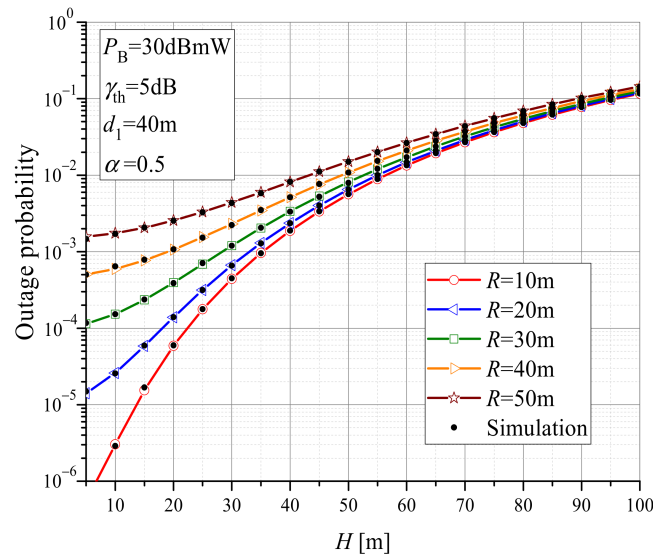


Figure 3. The outage probability dependence on the UAV height H and radius R .

The dependence of the outage probability on the distance between the PB and the sensor node is presented in Figure 4, for various values of time-switching coefficient α and various UAV heights. In this case the specific scenario is analyzed, where the total reachable distance from power beacon equal $d_1 + R$ remains constant. One can observe that the highest outage probability is obtained when distance d_1 and radius R are approximately equal, while smaller values are obtained when either PB-S distance or radius have small values. These results can show that a trade-off between these parameters can be achieved depending on the application. Further, for larger value of time-switching coefficient the outage probability decreases as sensor node is supplied with larger amount of energy and it is used within the correspondingly shorter interval, which results in the increased total sensor transmit power. In addition, for the case when the sensor is located closer to PB, the collected power is higher and the influence of height H on the outage performance is negligible. However, at longer PB-S distances, at low sensor transmitted power, performance degrades with increasing height.

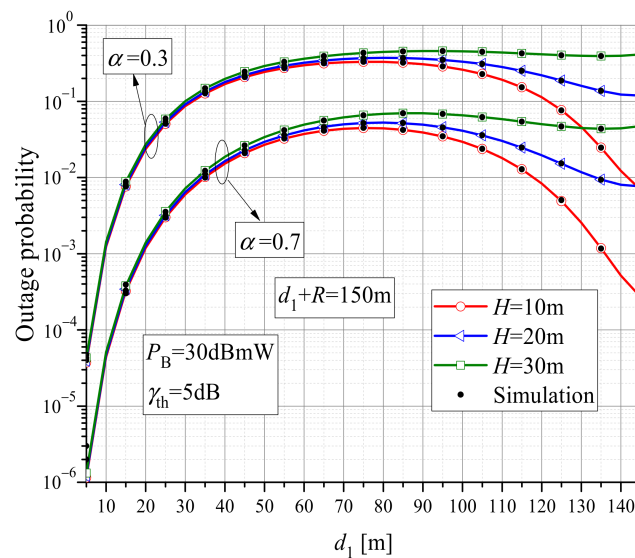


Figure 4. The outage probability dependence on the distance between the PB and S, $d_1 + R = 150$ m.

In Figure 5, the impact of the height H on the outage probability is investigated, for various values of the path loss coefficient ($\delta_2 = 2.7$ and $\delta_2 = 2$ for the free space environment)

and various values of fading parameter on S-to-UAV channels. We examined the case when $H + R = 50$ m and observed the effects of trade-off between H and R values. As is expected, higher values of path loss coefficient result in the increase of the outage probability. Furthermore, when the fading parameter m_2 increases, the fading severity of the S-to-UAV channel decreases, which further leads to better system performance. The results obtained by keeping the value of $H + R$ constant show that in this scenario there is an optimal value of H that leads to the minimum value of outage probability.

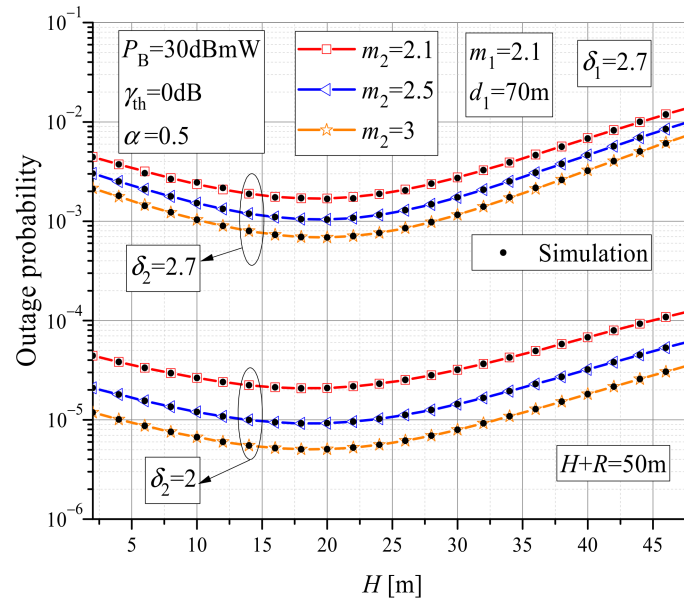


Figure 5. The outage probability dependence on the UAV height H and propagation parameters, $H + R = 50$ m.

The contour plots of outage probability are presented in Figure 6a,b, for the cases when $H + R = 50$ m and $d_1 + R = 100$ m, respectively. The influence of H and R values for the fixed sum $H + R = 50$ m shows the existence of maximum distance $d_{1,max}$ between the PB and the sensor node at a certain height H in order to obtain the defined value of outage probability. The trade-off between d_1 and R when $d_1 + R = 100$ m is presented in Figure 6b. Obtained results show that in order to obtain the outage probability smaller than 10^{-2} at distances $d_1 < 40$ m, the height H where the drone is positioned can be up to 40 m. However, at longer PB-to-S distances d_1 , the height H of UAV data collector should not exceed approximately 25 m to achieve an outage probability smaller than 10^{-2} .

The outage throughput is presented in Figure 7 as the function of the time-switching parameter α for various distances between the sensor node and the power beacon. It can be observed that the larger distance d_1 results in smaller outage throughput and higher value of optimal time-switching coefficient that maximizes throughput for the fixed remaining parameters.

The throughput T_{out} in the function of the time-switching parameter α is given in Figure 8, for various values of UAV altitude and various ratio of d_1 and R . For higher values of altitude H , when the sensor is closer to PB, it takes less time to charge the sensor, i.e., the maximum value of T_{out} is obtained for a smaller optimal value of time-switching coefficient. At lower altitudes ($H = 10$ m), throughput is higher due to the smaller distance d_2 , the sensor needs less energy to send information, so the optimal value of time-switching coefficient is smaller. Moreover, it can be seen in this case that a smaller value of R leads to larger value of throughput T_{out} .

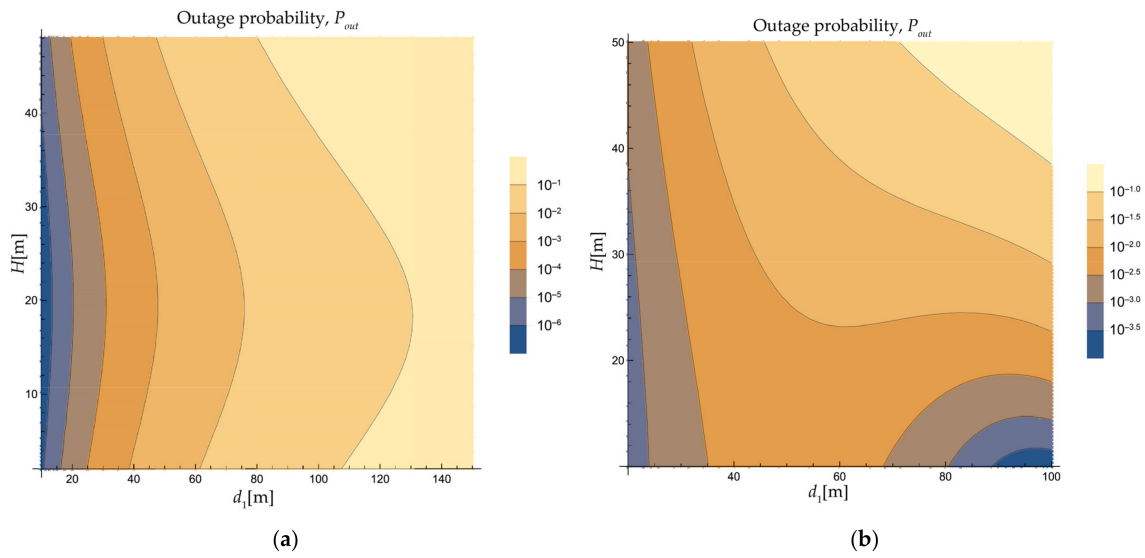


Figure 6. The dependence of outage probability on d_1 and H : (a) $H + R = 50$ m; (b) $d_1 + R = 100$ m.

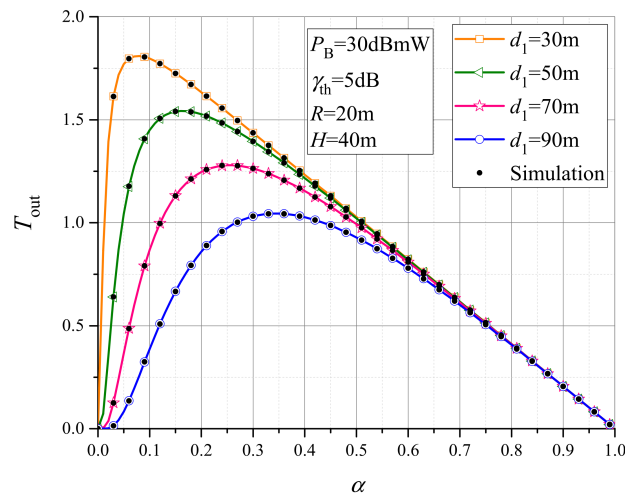


Figure 7. The outage throughput dependence on the time-switching coefficient α , for various values of d_1 .

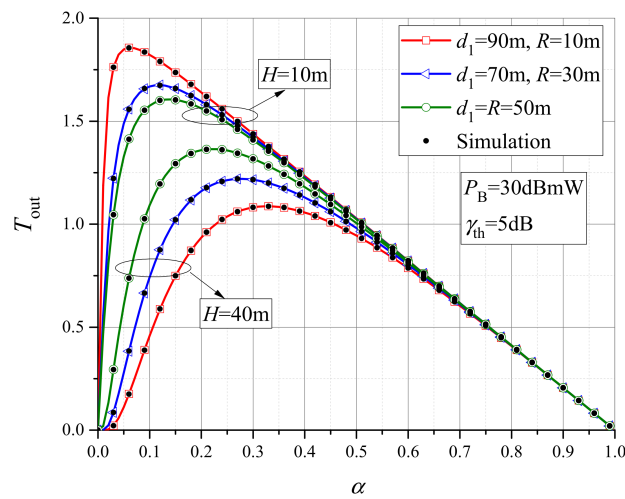


Figure 8. The outage throughput dependence on the time-switching coefficient α , for various values of H .

The ergodic throughput is presented in the contour Figure 9, as the function of time-switching coefficient α and distance d_1 . The analysis is done for the fixed sum $d_1 + R = 150$ m. The altitude of UAV data collector is set to 10 m. According to the obtained results, the trade-off between d_1 and R can make a large impact on the obtained system performances. Regardless of the system geometry, in order to ensure a throughput greater than 2 b/s/Hz, it is necessary to use the time-switching coefficient α in the range (0.2, 0.5). At small PB-to-sensor distances, i.e., d_1 less than 30 m (the UAV's coverage area is within the circle of radius $R > 120$ m), a throughput greater than 2 b/s/Hz is achieved when the sensor charging time is less than $0.8 T$. Moreover, the required throughput is achieved by reducing the radius R of the circular coverage area, and if the sensor is farther from the PB, the longer charging time compensates for the larger distance.

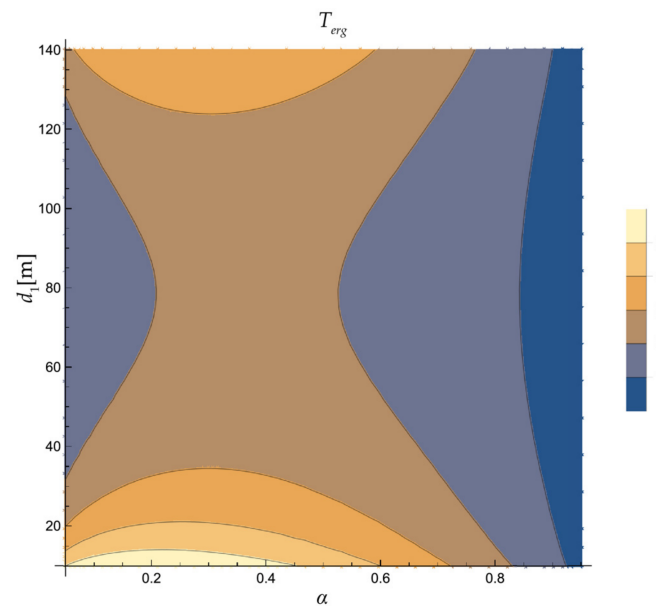


Figure 9. The ergodic throughput dependence on the time-switching coefficient α and d_1 , for $d_1 + R = 150$ m.

In Figure 10, the ergodic throughput is presented as the function of the time-switching coefficient α , and presented for various values of the path loss coefficient in the S-to-UAV channel. The results are also given for various values of UAV altitude H and the fixed sum $H + R = 50$ m. In accordance with the expectations, the higher values of ergodic throughput are achieved at lower UAV altitudes. The dependence of T_{erg} on the time-switching coefficient α is not straightforward, as larger value of α implies longer charging time and higher value of receive SNR at the UAV, but reduces the time dedicated for information transfer. The optimal value of time-switching coefficient that maximizes performances can be determined and in the observed scenario it is smaller for lower height H and path loss δ_2 values. Furthermore, the maximum throughput is achieved for a smaller time-switching coefficient α and UAV height values. This is a consequence of the smaller distance d_2 between the sensor and the UAV, but also a longer time dedicated for information transfer. For smaller values of α , the trade-off between H and R is clearly visible, while for larger values of α , the influence of the trade-off between H and R diminishes due to dominant influence of information transfer time $(1 - \alpha)T$.

Based on derived closed-form expressions for outage throughput (15) and ergodic throughput (19), optimal system parameters can be determined. By differentiating equation with respect to time-switching coefficient α and by equating it to zero, the optimal sensor charging time is numerically evaluated.

In Figure 11, optimal values of time-switching coefficient that maximizes outage throughput are obtained for different PB-to-sensor distance d_1 and fixed sum $d_1 + R = 100$ m.

The optimal charging times are calculated for different values of path loss exponent of sensor-to-UAV link and for various UAV altitudes. In the case of free space sensor-UAV environment ($\delta_1 = 2$), the impact of the height H on the optimal charging time is less significant when compared to the propagation environment with $\delta_2 = 2.7$. For low UAV altitude values equal to $H = 10$ m, the equal values of maximum throughput can be achieved for the same optimal value $\alpha_{opt} = 0.125$ and two different set of parameters, i.e., for $d_1 = 40$ m and $R = 60$ m and for $d_1 = 65$ m and $R = 35$ m. For the highest value of H , the optimal time-switching coefficient α_{opt} increases with the raise of distance d_1 .

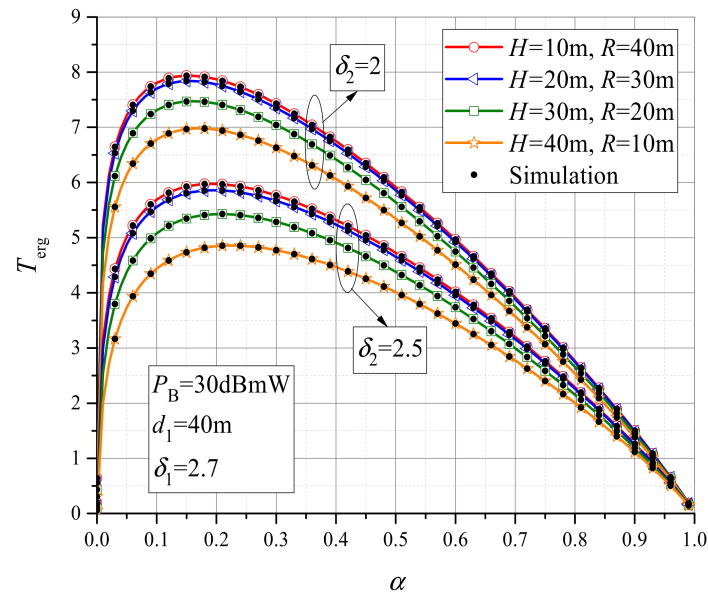


Figure 10. The ergodic throughput dependence on the time-switching coefficient α for various values of UAV altitude and path loss coefficient, for $H + R = 50$ m.

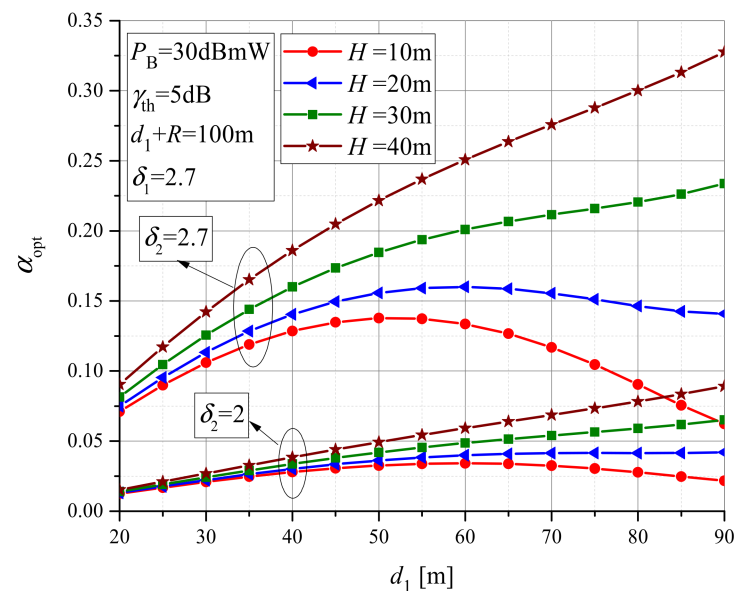


Figure 11. Optimal value of time-switching coefficient α for outage throughput, for various values of UAV altitude and the sensor-to-UAV path loss coefficient, $d_1 + R = 100$ m.

The values of sensor charging time for achieving maximal ergodic throughput are presented in Figure 12. Results are obtained for various values of the path loss exponents in the PB-to-sensor and the sensor-to-UAV link, while UAV altitude is varied for the constant

sum $H + R = 50$ m. In accordance with the expectations, the optimal time-switching coefficient α_{opt} is increasing with the raise of H . Practically, the corresponding charging time of the sensor is rising in that case. The optimal value α_{opt} reaches its minimum for the smaller value of H , when charging can be shortened due to smaller PB-to-sensor distances. The increase of the path loss in the PB-to-sensor link leads to longer charging time.

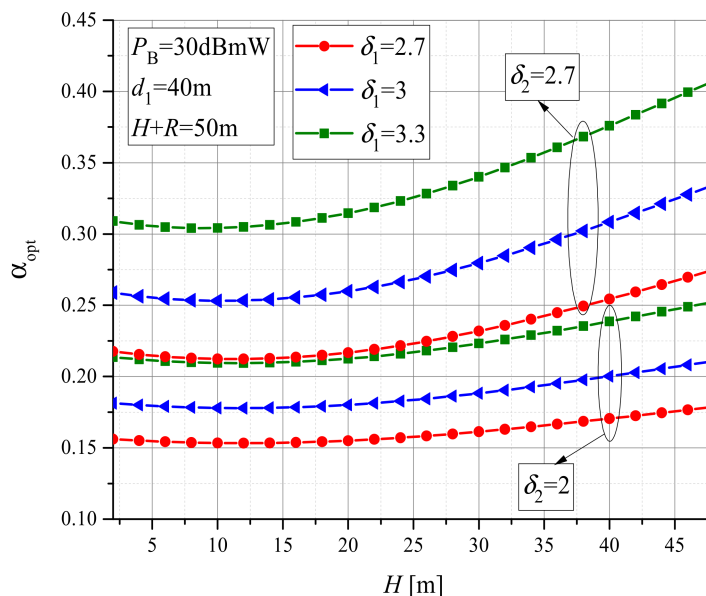


Figure 12. Optimal value of time-switching coefficient for ergodic throughput, for various values of path loss coefficients, $H + R = 50$ m.

5. Conclusions

In this paper we analyzed the performance of an industrial IoT system where the energy-constrained node is assisted with a power beacon. The data collection is based on UAVs, as the IoT node is positioned in an inaccessible location with no available communication infrastructure. We have derived the closed-form results for the outage probability, the outage capacity and the ergodic capacity of the system, taking into account the randomness of the UAV position within a circle of a certain radius. The correctness of the derived analytical expressions is verified by an independent simulation method.

Based on the presented results, we have investigated the influence of the channel parameters on the system performance, as well as the impact of system parameters such as the energy harvesting time-switching ratio, area coverage size, UAV height and UAV distance from the power beacon. The provided analysis represents the basis for determining parameters adequate for the environment where the system is realized with possible limitations, as targeted throughput performances can be obtained with different system parameters. Based on the analysis, the optimal sensor charging time values that maximize the outage throughput as well the ergodic throughput are determined. The influence of the charging time (i.e., the time-switching coefficient) on the obtainable outage and ergodic throughput is twofold. The longer charging implies higher accumulated energy at the sensor and larger SNR values at the UAV, but lowers the time dedicated for information transfer and corresponding obtainable throughput. The obtained results show that the optimal time-switching coefficient is higher for larger distances d_1 from the power beacon and larger UAV heights H , as the needed charging time is longer due to larger path losses. However, the obtainable throughput in these cases is lower. When the sum of UAV height and radius of UAV movement is considered to be constant, the ergodic capacity is lower for a higher height H . The obtained results can be a valuable guideline for the design of industrial systems without any available communication infrastructure, in the design of the

systems affected by natural disasters and data acquisition systems for monitoring critical toxic parameters.

Author Contributions: Conceptualization, A.C. and V.B.; methodology, A.C. and V.B.; software, A.C.; validation, A.C. and V.B.; formal analysis, A.C. and V.B.; investigation, A.C. and V.B.; resources, A.C., V.B. and J.M.; data curation, A.C.; writing—original draft preparation, A.C. and V.B.; writing—review and editing, A.C., V.B. and J.M.; visualization, V.B.; supervision, A.C., V.B. and J.M.; project administration, A.C. and V.B.; funding acquisition, A.C., V.B. and J.M. All authors have read and agreed to the published version of the manuscript.

Funding: This research received no external funding.

Data Availability Statement: Not applicable.

Acknowledgments: The work of A. Cvetkovic and J. Manojlovic was partly financially supported by the Ministry of Education, Science and Technological Development of the Republic of Serbia (Contract No. 451-03-68/2022-14/ 200109). Vesna Blagojevic acknowledges the support of the Science Fund of the Republic of Serbia, grant No 7750284 (Hybrid Integrated Satellite and Terrestrial Access Network—hi-STAR).

Conflicts of Interest: The authors declare no conflict of interest.

Appendix A

By substituting (8) and (9) in (10), we obtain

$$p_{UAV}(\gamma) = \frac{4}{\Gamma(m_1)\Gamma(m_2)R^2} \left(\frac{(1-\alpha)m_1m_2d_1^{\delta_1}\sigma^2}{\bar{\gamma}_1\bar{\gamma}_2\eta\alpha P_B} \right)^{\frac{m_1+m_2}{2}} \gamma^{\frac{m_1+m_2}{2}-1} \times \int_0^R (H^2+r^2)^{\frac{\delta_2(m_1+m_2)}{4}} K_{-m_1+m_2} \left(2\sqrt{\frac{(1-\alpha)m_1m_2d_1^{\delta_1}(H^2+r^2)^{\delta_2/2}\sigma^2\gamma}{\bar{\gamma}_1\bar{\gamma}_2\eta\alpha P_B}} \right) r dr. \tag{A1}$$

To find a closed-form expression for the PDF of the SNR at the UAV, in the following integral

$$I = \int_0^R (H^2+r^2)^{\frac{\delta_2(m_1+m_2)}{4}} K_{-m_1+m_2} \left(2\sqrt{\frac{(1-\alpha)m_1m_2d_1^{\delta_1}(H^2+r^2)^{\delta_2/2}\sigma^2\gamma}{\bar{\gamma}_1\bar{\gamma}_2\eta\alpha P_B}} \right) r dr, \tag{A2}$$

we introduce a change of variables $y = (H^2+r^2)^{\frac{\delta_2}{2}}$. Further, we obtain

$$I = \frac{2}{\delta_2 R^2} \int_{H^{\delta_2}}^{(H^2+R^2)^{\frac{\delta_2}{2}}} y^{\frac{m_1+m_2}{2}-1+\frac{2}{\delta_2}} K_{-m_1+m_2} \left(2\sqrt{\frac{(1-\alpha)m_1m_2d_1^{\delta_1}\sigma^2\gamma}{\bar{\gamma}_1\bar{\gamma}_2\eta\alpha P_B}} y \right) dy. \tag{A3}$$

By using the transformation of modified Bessel function of the second kind into Meijer’s G-function [48] (03.04.26.0008.01), the integral I can be further expressed as

$$I = \frac{1}{\delta_2 R^2} \int_{H^{\delta_2}}^{(H^2+R^2)^{\frac{\delta_2}{2}}} y^{\frac{m_1+m_2}{2}-1+\frac{2}{\delta_2}} G_{0,2}^{2,0} \left(\frac{(1-\alpha)m_1m_2d_1^{\delta_1}\sigma^2\gamma}{\bar{\gamma}_1\bar{\gamma}_2\eta\alpha P_B} y \mid \begin{matrix} - \\ \frac{m_2-m_1}{2}, \frac{m_1-m_2}{2} \end{matrix} \right) dy \\ = \frac{1}{\delta_2 R^2} \int_0^{(H^2+R^2)^{\frac{\delta_2}{2}}} y^{\frac{m_1+m_2}{2}-1+\frac{2}{\delta_2}} G_{0,2}^{2,0} \left(\frac{(1-\alpha)m_1m_2d_1^{\delta_1}\sigma^2\gamma}{\bar{\gamma}_1\bar{\gamma}_2\eta\alpha P_B} y \mid \begin{matrix} - \\ \frac{m_2-m_1}{2}, \frac{m_1-m_2}{2} \end{matrix} \right) dy \\ - \frac{1}{\delta_2 R^2} \int_0^{H^{\delta_2}} y^{\frac{m_1+m_2}{2}-1+\frac{2}{\delta_2}} G_{0,2}^{2,0} \left(\frac{(1-\alpha)m_1m_2d_1^{\delta_1}\sigma^2\gamma}{\bar{\gamma}_1\bar{\gamma}_2\eta\alpha P_B} y \mid \begin{matrix} - \\ \frac{m_2-m_1}{2}, \frac{m_1-m_2}{2} \end{matrix} \right) dy. \tag{A4}$$

Then, applying [48] (07.34.21.0084.01) the closed-form solution for I is obtained

$$\begin{aligned}
 I &= \frac{1}{\delta_2 R^2} \frac{1}{(H^2 + R^2)^{-\frac{\delta_2}{2} \left(\frac{m_1 + m_2}{2} + \frac{2}{\delta_2} \right)}} \\
 &\times G_{1,3}^{2,1} \left(\frac{(1-\alpha)m_1 m_2 d_1^{\delta_1} \sigma^2 \gamma}{\tilde{\gamma}_1 \tilde{\gamma}_2 \eta \alpha P_B} (H^2 + R^2)^{\frac{\delta_2}{2}} \left| \frac{1 - \frac{m_1 + m_2}{2} - \frac{2}{\delta_2}}{\frac{m_2 - m_1}{2}, \frac{m_1 - m_2}{2}, -\frac{m_1 + m_2}{2} - \frac{2}{\delta_2}} \right. \right) \\
 &- \frac{1}{\delta_2 R^2} \frac{1}{H^{-\delta_2 \left(\frac{m_1 + m_2}{2} + \frac{2}{\delta_2} \right)}} \\
 &\times G_{1,3}^{2,1} \left(\frac{(1-\alpha)m_1 m_2 d_1^{\delta_1} \sigma^2 \gamma}{\tilde{\gamma}_1 \tilde{\gamma}_2 \eta \alpha P_B} H^{\delta_2} \left| \frac{1 - \frac{m_1 + m_2}{2} - \frac{2}{\delta_2}}{\frac{m_2 - m_1}{2}, \frac{m_1 - m_2}{2}, -\frac{m_1 + m_2}{2} - \frac{2}{\delta_2}} \right. \right). \quad (A5)
 \end{aligned}$$

By substituting (A5) in (A1) the closed-form PDF is derived and presented in expression (11).

References

- Popescu, D.; Stoican, F.; Stamatescu, G.; Chenaru, O.; Ichim, L. A Survey of Collaborative UAV-WSN Systems for Efficient Monitoring. *Sensors* **2019**, *19*, 4690. [CrossRef] [PubMed]
- Rameshkumar, C.; Ganeshkumar, T. A Novel of Survey: In Healthcare System for Wireless Body-Area Network. In *Applications of Computational Methods in Manufacturing and Product Design*; Deepak, B.B.V.L., Parhi, D., Biswal, B., Jena, P.C., Eds.; Springer: Singapore, 2022; pp. 591–609. [CrossRef]
- Yaghoubi, M.; Ahmed, K.; Miao, Y. Wireless Body Area Network (WBAN): A Survey on Architecture, Technologies, Energy Consumption, and Security Challenges. *J. Sens. Actuator Netw.* **2022**, *11*, 67. [CrossRef]
- Lanzolla, A.; Spadavecchia, M. Wireless Sensor Networks for Environmental Monitoring. *Sensors* **2021**, *21*, 1172. [CrossRef] [PubMed]
- Majid, M.; Habib, S.; Javed, A.R.; Rizwan, M.; Srivastava, G.; Gadekallu, T.R.; Lin, J.C.-W. Applications of Wireless Sensor Networks and Internet of Things Frameworks in the Industry Revolution 4.0: A Systematic Literature Review. *Sensors* **2022**, *22*, 2087. [CrossRef]
- Compare, M.; Baraldi, P.; Zio, E. Challenges to IoT-Enabled Predictive Maintenance for Industry 4.0. *IEEE Internet Things J.* **2020**, *7*, 4585–4597. [CrossRef]
- Malik, P.K.; Sharma, R.; Singh, R.; Gehlot, A.; Satapathy, S.C.; Alnumay, W.S.; Pelusi, D.; Ghosh, U.; Nayak, J. Industrial Internet of Things and its Applications in Industry 4.0: State of The Art. *Comput. Commun.* **2021**, *166*, 125–139. [CrossRef]
- Liu, Y.; Ma, X.; Shu, L.; Hancke, G.P.; Abu-Mahfouz, A.M. From Industry 4.0 to Agriculture 4.0: Current Status, Enabling Technologies, and Research Challenges. *IEEE Trans. Industr. Inform.* **2021**, *17*, 4322–4334. [CrossRef]
- Oztemel, E.; Gursev, S. Literature Review of Industry 4.0 and Related Technologies. *J. Intell. Manuf.* **2020**, *31*, 127–182. [CrossRef]
- Prauzek, M.; Konecny, J.; Borova, M.; Janosova, K.; Hlavica, J.; Musilek, P. Energy Harvesting Sources, Storage Devices and System Topologies for Environmental Wireless Sensor Networks: A Review. *Sensors* **2018**, *18*, 2446. [CrossRef]
- Huda, S.M.A.; Arafat, M.Y.; Moh, S. Wireless Power Transfer in Wirelessly Powered Sensor Networks: A Review of Recent Progress. *Sensors* **2022**, *22*, 2952. [CrossRef]
- Masotti, D.; Shanawani, M.; Murtaza, G.; Paolini, G.; Costanzo, A. RF Systems Design for Simultaneous Wireless Information and Power Transfer (SWIPT) in Automation and Transportation. *IEEE J. Microw.* **2021**, *1*, 164–175. [CrossRef]
- Costanzo, A.; Masotti, D.; Paolini, G.; Schreurs, D. Evolution of SWIPT for the IoT World: Near- and Far-Field Solutions for Simultaneous Wireless Information and Power Transfer. *IEEE Microw. Mag.* **2021**, *22*, 48–59. [CrossRef]
- Phan, V.D.; Nguyen, T.N.; Tran, M.; Trang, T.T.; Voznak, M.; Ha, D.H.; Nguyen, T.L. Power Beacon-Assisted Energy Harvesting in a Half-Duplex Communication Network under Co-channel Interference over a Rayleigh Fading Environment: Energy Efficiency and Outage Probability Analysis. *Energies* **2019**, *12*, 2579. [CrossRef]
- Verma, G.; Sharma, V. A Novel RF Energy Harvester for Event-Based Environmental Monitoring in Wireless Sensor Networks. *IEEE Internet Things J.* **2022**, *9*, 3189–3203. [CrossRef]
- Choi, H.-H.; Lee, J.-R. Energy-Neutral Operation Based on Simultaneous Wireless Information and Power Transfer for Wireless Powered Sensor Networks. *Energies* **2019**, *12*, 3823. [CrossRef]
- Le, C.B.; Nguyen, N.D. Enabling Power Beacons and Wireless Power Transfers for Non-Orthogonal Multiple Access Networks. *J. Telecommun. Inf. Technol.* **2021**, *3*, 1. [CrossRef]
- Zhou, X.; Guo, J.; Durrani, S.; Di Renzo, M. Power Beacon-Assisted Millimeter Wave Ad Hoc Networks. *IEEE Trans. Commun.* **2018**, *66*, 830–844. [CrossRef]
- Elshrkasi, A.; Dimiyati, K.; Ahmad, K.A.B.; Abdullah, E. Employing an Energy Harvesting Strategy to Enhance the Performance of a Wireless Emergency Network. *Sensors* **2022**, *22*, 4385. [CrossRef]
- Nguyen, M.T.; Nguyen, C.V.; Do, H.T.; Hua, H.T.; Tran, T.A.; Nguyen, A.D.; Ala, G.; Viola, F. UAV-assisted Data Collection in Wireless Sensor Networks: A Comprehensive Survey. *Electronics* **2021**, *10*, 2603. [CrossRef]

21. Noor, F.; Khan, M.A.; Al-Zahrani, A.; Ullah, I.; Al-Dhlan, K.A. A Review on Communications Perspective of Flying Ad-Hoc Networks: Key Enabling Wireless Technologies, Applications, Challenges and Open Research Topics. *Drones* **2020**, *4*, 65. [[CrossRef](#)]
22. Shah, A.F.M.S. Architecture of Emergency Communication Systems in Disasters through UAVs in 5G and Beyond. *Drones* **2023**, *7*, 25. [[CrossRef](#)]
23. Azam, I.; Shahab, M.B.; Shin, S.Y. Energy-Efficient Pairing and Power Allocation for NOMA UAV Network Under QoS Constraints. *IEEE Internet Things J.* **2022**, *9*, 25011–25026. [[CrossRef](#)]
24. Liu, X.; Li, Z.; Zhao, N.; Meng, W.; Gui, G.; Chen, Y.; Adachi, F. Transceiver Design and Multihop D2D for UAV IoT Coverage in Disasters. *IEEE Internet Things J.* **2019**, *6*, 1803–1815. [[CrossRef](#)]
25. Bithas, P.S.; Nikolaidis, V.; Kanatas, A.G.; Karagiannidis, G.K. UAV-to-Ground Communications: Channel Modeling and UAV Selection. *IEEE Trans Commun.* **2020**, *68*, 5135–5144. [[CrossRef](#)]
26. Khuwaja, A.A.; Chen, Y.; Zheng, G. Effect of User Mobility and Channel Fading on the Outage Performance of UAV Communications. *IEEE Wireless Commun. Lett.* **2020**, *9*, 367–370. [[CrossRef](#)]
27. Sharma, P.K.; Deepthi, D.; Kim, D.I. Outage Probability of 3-D Mobile UAV Relaying for Hybrid Satellite-Terrestrial Networks. *IEEE Commun. Lett.* **2020**, *24*, 418–422. [[CrossRef](#)]
28. Sarfraz, M.; Sohail, M.F.; Alam, S.; Javvad ur Rehman, M.; Ghauri, S.A.; Rabie, K.; Abbas, H.; Ansari, S. Capacity Optimization of Next-Generation UAV Communication Involving Non-Orthogonal Multiple Access. *Drones* **2022**, *6*, 234. [[CrossRef](#)]
29. Nguyen, A.-N.; Vo, V.N.; So-In, C.; Ha, D.-B. System Performance Analysis for an Energy Harvesting IoT System Using a DF/AF UAV-Enabled Relay with Downlink NOMA under Nakagami- m Fading. *Sensors* **2021**, *21*, 285. [[CrossRef](#)]
30. Hoseini, S.A.; Hassan, J.; Bokani, A.; Kanhere, S.S. In Situ MIMO-WPT Recharging of UAVs Using Intelligent Flying Energy Sources. *Drones* **2021**, *5*, 89. [[CrossRef](#)]
31. Ji, B.; Li, Y.; Zhou, B.; Li, C.; Song, K.; Wen, H. Performance Analysis of UAV Relay Assisted IoT Communication Network Enhanced With Energy Harvesting. *IEEE Access* **2019**, *7*, 38738–38747. [[CrossRef](#)]
32. Tran, D.H.; Nguyen, V.D.; Chatzinotas, S.; Vu, T.X.; Ottersten, B. UAV Relay-Assisted Emergency Communications in IoT Networks: Resource Allocation and Trajectory Optimization. *IEEE Trans. Wirel. Commun.* **2022**, *21*, 1621–1637. [[CrossRef](#)]
33. Singh, S.K.; Agrawal, K.; Singh, K.; Li, C.-P. Outage Probability and Throughput Analysis of UAV-Assisted Rate-Splitting Multiple Access. *IEEE Wireless Commun. Lett.* **2021**, *10*, 2528–2532. [[CrossRef](#)]
34. Zhang, J.; Chuai, G.; Gao, W. Energy-Efficient Optimization for Energy-Harvesting-Enabled mmWave-UAV Heterogeneous Networks. *Entropy* **2022**, *24*, 300. [[CrossRef](#)]
35. Liu, Y.; Dai, H.N.; Wang, H.; Imran, M.; Wang, X.; Shoaib, M. UAV-enabled Data Acquisition Scheme with Directional Wireless Energy Transfer for Internet of Things. *Comput. Commun.* **2020**, *155*, 184–196. [[CrossRef](#)]
36. Lei, H.; Wang, D.; Park, K.H.; Ansari, I.S.; Jiang, J.; Pan, G.; Alouini, M.S. Safeguarding UAV IoT Communication Systems Against Randomly Located Eavesdroppers. *IEEE Internet Things J.* **2020**, *7*, 1230–1244. [[CrossRef](#)]
37. Aiello, G.; Hopps, F.; Santisi, D.; Venticinque, M. The Employment of Unmanned Aerial Vehicles for Analyzing and Mitigating Disaster Risks in Industrial Sites. *IEEE Trans. Eng. Manag.* **2022**, *67*, 519–530. [[CrossRef](#)]
38. Fotouhi, A.; Qiang, H.; Ding, M.; Hassan, M.; Giordano, L.G.; Garcia-Rodriguez, A.; Yuan, J. Survey on UAV Cellular Communications: Practical Aspects, Standardization Advancements, Regulation, and Security Challenges. *IEEE Commun. Surv. Tutor.* **2019**, *21*, 3417–3442. [[CrossRef](#)]
39. Yacoub, M.D.; Bautista, J.V.; de Rezende Guedes, L.G. On Higher Order Statistics of the Nakagami- m Distribution. *IEEE Trans. Veh. Technol.* **1999**, *48*, 790–794. [[CrossRef](#)]
40. Goldsmith, A. *Wireless Communications*; Cambridge University Press: Cambridge, UK, 2005.
41. Zhang, Y.; Ye, J.; Pan, G.; Alouini, M.S. Secrecy Outage Analysis for Satellite-Terrestrial Downlink Transmissions. *IEEE Wireless Commun. Lett.* **2020**, *9*, 1643–1647. [[CrossRef](#)]
42. Boschiero, M.; Giordani, M.; Polese, M.; Zorzi, M. Coverage Analysis of UAVs in Millimeter Wave Networks: A stochastic Geometry Approach. In Proceedings of the 2020 International Wireless Communications and Mobile Computing (IWCMC), Limassol, Cyprus, 15–19 June 2020.
43. Gu, Y.; Aissa, S. RF-Based Energy Harvesting in Decode-and-Forward Relaying Systems: Ergodic and Outage Capacities. *IEEE Trans. Wirel. Commun.* **2015**, *14*, 6425–6434. [[CrossRef](#)]
44. Gradshteyn, I.S.; Ryzhik, I.M. *Table of Integrals, Series, and Products*, 7th ed.; Elsevier/Academic Press: London, UK, 2007.
45. Papoulis, A. *Probability, Random Variables, and Stochastic Processes*; McGraw-Hill: New York, NY, USA, 1991.
46. Karagiannidis, G.K.; Sagiias, N.C.; Mathiopoulos, P.T. N* Nakagami: A Novel Stochastic Model for Cascaded Fading Channels. *IEEE Trans. Commun.* **2007**, *55*, 1453–1458. [[CrossRef](#)]
47. Shankar, P.M. *Fading and Shadowing in Wireless Systems*; Springer: New York, NY, USA, 2012.
48. Wolfram Research. Available online: <https://functions.wolfram.com/> (accessed on 20 October 2022).

Disclaimer/Publisher’s Note: The statements, opinions and data contained in all publications are solely those of the individual author(s) and contributor(s) and not of MDPI and/or the editor(s). MDPI and/or the editor(s) disclaim responsibility for any injury to people or property resulting from any ideas, methods, instructions or products referred to in the content.